

Supplementary Information to:
*Dynamical regulation in bacterial cells during
steady-state growth*

M. Wehrens*, L.H.J. Krah*, B.D. Towbin, R. Hermsen, S.J. Tans

December 9, 2021

Contents

1 Mathematical analysis of the noise model	2
1.1 Model definition and parameter interpretation	2
1.2 Metabolic timescale, solution in Fourier space	4
1.3 Calculated variances and cross-covariances	5
1.3.1 Definition of cross-covariance	5
1.3.2 Analytical expressions for the coefficients of variation	5
1.3.3 Analytical expressions for the cross-covariances	6
1.3.4 Functional forms of the building blocks	7
2 Analysing the cross-correlations	9
2.1 Old decomposition	9
2.2 C-sector cross-correlation: New decomposition	9
2.3 Summary of the new decomposition for the reporters	10
2.3.1 C-sector reporter concentration	10
2.3.2 C-sector reporter production rate	11
2.3.3 Constitutive reporter concentration	11
2.3.4 Constitutive reporter production rate	11
2.4 New decomposition example	11
3 Parameter reduction	12
4 Data analysis	15
4.1 Calculating cross-correlations from data	15
4.2 Averaging multiple experiments and estimating error bars	15
4.3 Null-expectation for the cross-correlations	16
5 Fitting procedure	17
5.1 Wild type and cAMP-fixed* cells	17
6 Toy model of the means of the two reporters	19
7 Supplementary Figures	21

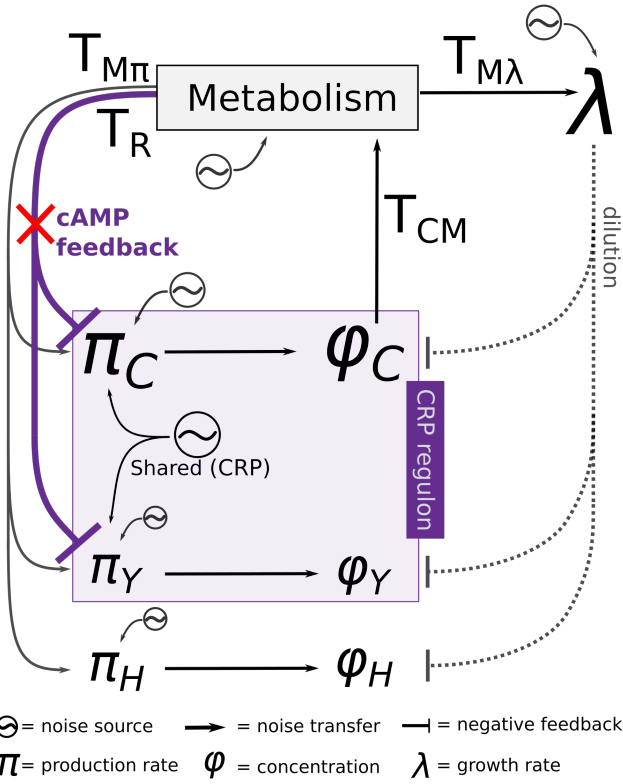


Figure S1: Diagram of the Noise Routes, including C reporter (Y) and constitutive reporter (H). An additional shared noise source is added between π_C and π_Y , here called N_s , that represents noise in the sensory mechanism (here they could be CRP-concentration fluctuations, for example). The transfer from Metabolism (M) to production exist of the sum of general transfer ($T_{M\pi}$) and regulatory transfer (T_R), which only acts on the C-sector and its reporter, Y.

1 Mathematical analysis of the noise model

Note on notation: Where the main text talks about the C-sector reporter (CRPr) and the not CRP-regulated constitutive reporter (nCRPr), this document uses the notation ‘Y’ for the C-sector reporter and ‘H’ for the constitutive reporter.

1.1 Model definition and parameter interpretation

Similar to Kiviet *et al.* [1] a linear noise propagation model can be constructed using the diagram of Fig. S1. The model captures the interplay between the production rate (π) of certain proteins, the concentrations (ϕ) of these proteins, metabolism (M) and the growth rate (λ).

We model the total C-sector in a coarse-grained manner as a single protein, C, whose fluctuations directly influence (the rate of) metabolism. Additionally, we model the two fluorescent reporters, for ease of notation here called Y and H, that are not metabolically active and hence do not control metabolism.

We assume that the variables fluctuate around a particular average state $\{\lambda_0, M_0, \vec{\pi}_0, \vec{\phi}_0\}$; the model describes the dynamics of small, relative deviations of each variable from its respective

average, $\frac{\delta X(t)}{X_0} := \frac{X(t) - X_0}{X_0}$. (Below, the explicit time dependence will often be omitted.) These deviations, referred to as “noise”, propagate through the system according to the arrows in Fig. S1. For example, fluctuations in the production rate π_C affect ϕ_C , whose fluctuations affect M . Via M the noise then further transfers to the production rates and to the growth rate. Noise in the growth rate in turn affects the dilution of all proteins (dashed line). The logarithmic gains/transfer coefficients T_{AB} describe the strength of noise propagation from A to B .

The role for metabolism is crucial in our model because many noise routes pass through metabolism, but also because the cAMP-CRP regulatory network reacts to metabolic fluctuations. The interpretation of M is therefore not straightforward. M could be interpreted as the rate of metabolism. However, we assume that with a higher rate of metabolism, the concentrations of certain internal metabolites (in particular keto-acids such as OAA) also increase. The metabolite OAA is known to inhibit the production of cAMP in wild type cells [2] (see Fig. 1A of the main text), therewith triggering the cAMP-CRP regulatory feedback when M increases (represented by the regulatory parameter T_R in the model, Fig. S1). Although we model metabolism with a single variable M , it thus represents both the rate of metabolism and the saturation level of metabolic precursors such as OAA.

Certain variables are directly influenced by phenomenological, independent coloured noise sources, denoted as N_i : Ornstein–Uhlenbeck Noise sources that each have a specific timescale. These noise sources offer a way to model the combined effect of many stochastic processes that together influence the dynamics of certain variables. For example, N_{π_Y} summarises processes that intrinsically influence the production rate of the Y reporter, such as transcription and translation. N_M , the noise source acting on metabolism, is primarily the result of fluctuations in the concentration of individual protein species that are part of the C-sector. The fluctuations of all these proteins together are expected to cause the metabolic flux to fluctuate, even if the total size of the C-sector is roughly constant. Fluctuations in the concentrations of individual proteins are diluted via growth, so that the N_M noise source has a timescale close to λ_0 . N_λ has a similar interpretation. N_s is a shared noise source between the C-sector and the C-sector reporter Y , mainly interpreted as fluctuations in the production of CRP-regulated proteins due to fluctuations in the concentration of CRP itself. Even when the cAMP concentration is experimentally kept fixed in the mutant strain, fluctuations in the CRP concentration are expected to influence the cAMP-CRP concentration and therewith the production rate of both the C-sector and its reporter Y .

Based on the considerations above, we arrive at the following set of equations:

$$\frac{\delta\lambda}{\lambda_0} = N_\lambda + T_{M\lambda} \frac{\delta M}{M_0}, \quad (1)$$

$$\frac{\delta M}{M_0} = N_M + T_{CM} \frac{\delta\phi_C}{\phi_{C,0}}, \quad (2)$$

$$\frac{\delta\pi_C}{\pi_{0,C}} = N_{\pi_C} + N_s + (T_{M\pi} + T_R) \frac{\delta M}{M_0}, \quad (3)$$

$$\frac{\delta\pi_Y}{\pi_{0,Y}} = N_{\pi_Y} + N_s + (T_{M\pi} + T_R) \frac{\delta M}{M_0}, \quad (4)$$

$$\frac{\delta\pi_H}{\pi_{0,H}} = N_{\pi_H} + T_{M\pi} \frac{\delta M}{M_0}, \quad (5)$$

$$\left(\frac{\delta\dot{\phi}_C}{\lambda_0\phi_{0,C}} \right) = \frac{\delta\pi_C}{\pi_{0,C}} - \frac{\delta\phi_C}{\phi_{0,C}} - \frac{\delta\lambda}{\lambda_0}, \quad (6)$$

$$\left(\frac{\delta\dot{\phi}_Y}{\lambda_0\phi_{0,Y}} \right) = \frac{\delta\pi_Y}{\pi_{0,Y}} - \frac{\delta\phi_Y}{\phi_{0,Y}} - \frac{\delta\lambda}{\lambda_0}, \quad (7)$$

$$\left(\frac{\delta\dot{\phi}_H}{\lambda_0\phi_{0,H}} \right) = \frac{\delta\pi_H}{\pi_{0,H}} - \frac{\delta\phi_H}{\phi_{0,H}} - \frac{\delta\lambda}{\lambda_0}. \quad (8)$$

The last three equations are linearisations of the time derivative of the protein concentrations ($\dot{\phi}_i = \pi_i - \lambda\phi_i$), see also [1]. The dynamics of each noise source N_x is given by its stochastic differential equation,

$$dN_x = -\beta_x N_x dt + \theta_x dW_t, \quad (9)$$

where β_x is the noise source's timescale, θ_x its amplitude, and $W(t)$ a Wiener Process.

1.2 Metabolic timescale, solution in Fourier space

The system of equations 1-8 above can be solved in Fourier space. For each variable $A(t)$ we denote the Fourier Transform of $\delta A(t)$ as $\tilde{A}(\omega)$. Next, we introduce a metabolic timescale that scales with the mean growth rate: $\lambda_E = \lambda_0(1 - T_{CM}T_{MC})$, where $T_{MC} = T_R + T_{M\pi} - T_{M\lambda}$. This timescale can be interpret as the time it takes before the protein concentration equilibrates with its protein production rate (note that producing proteins takes time, such that a higher production rate now, only results in a higher concentration some time later). During exponential growth, proteins are generally produced at a (mean) rate proportional to λ_0 , such that production and dilution are balanced. In effect, fluctuations in protein concentrations generally decay on a timescale of λ_0 . However, in the case of C-sector proteins, synthesised proteins directly influence the rate of metabolism ($T_{CM} \neq 0$), and (depending on the parameters $T_R, T_{M\pi}$ and $T_{M\lambda}$) metabolism in turn influences the production rate and protein concentration. This changes the timescale of C-sector fluctuations from λ_0 to λ_E . Using this notation, we solve the linear system on the previous page in Fourier Space and arrive at:

$$\begin{cases} \frac{\widetilde{\delta\lambda}}{\lambda_0} &= N_\lambda + T_{M\lambda}N_M + \frac{\lambda_0}{\lambda_E+i\omega}(T_{CM}T_{M\lambda}) \left[N_{\pi_C} + N_s + T_{MC}N_M - N_\lambda \right], \\ \frac{\widetilde{\delta\phi_C}}{\phi_{C,0}} &= \frac{\lambda_0}{\lambda_E+i\omega} \left[N_{\pi_C} + N_s + T_{MC}N_M - N_\lambda \right], \\ \frac{\widetilde{\delta\pi_C}}{\pi_{C,0}} &= N_{\pi_C} + N_s + (T_R + T_{M\pi})N_M + \frac{\lambda_0}{\lambda_E+i\omega}T_{CM}(T_R + T_{M\pi}) \left[N_{\pi_C} + N_s + T_{MC}N_M - N_\lambda \right]. \end{cases} \quad (10)$$

$$\begin{cases} \widetilde{\frac{\delta\phi_Y}{\phi_{Y,0}}} &= \frac{\lambda_0}{\lambda_0+i\omega} \left[N_{\pi_Y} + N_s + T_{MC}N_M - N_\lambda \right] + \frac{\lambda_0^2 T_{CM}T_{MC}}{(\lambda_E+i\omega)(\lambda_0+i\omega)} \left[N_{\pi_C} + N_s + T_{MC}N_M - N_\lambda \right], \\ \widetilde{\frac{\delta\pi_Y}{\pi_{Y,0}}} &= N_{\pi_Y} + N_s + (T_R + T_{M\pi})N_M + \frac{\lambda_0}{\lambda_E+i\omega} T_{CM} (T_R + T_{M\pi}) \left[N_{\pi_C} + N_s + T_{MC}N_M - N_\lambda \right]. \end{cases} \quad (11)$$

$$\begin{cases} \widetilde{\frac{\delta\phi_H}{\phi_{H,0}}} &= \frac{\lambda_0}{\lambda_0+i\omega} \left[N_{\pi_H} + (T_{M\pi} - T_{M\lambda})N_M - N_\lambda \right] + \frac{\lambda_0^2 T_{CM}(T_{M\pi} - T_{M\lambda})}{(\lambda_E+i\omega)(\lambda_0+i\omega)} \left[N_{\pi_C} + N_s + T_{MC}N_M - N_\lambda \right], \\ \widetilde{\frac{\delta\pi_H}{\pi_{H,0}}} &= N_{\pi_H} + T_{M\pi}N_M + \frac{\lambda_0}{\lambda_E+i\omega} T_{CM}T_{M\pi} \left[N_{\pi_C} + N_s + T_{MC}N_M - N_\lambda \right]. \end{cases} \quad (12)$$

1.3 Calculated variances and cross-covariances

1.3.1 Definition of cross-covariance

The solution in Fourier Space (Eqs. 10 - 12) can be used to calculate variances and cross-covariances of the variables. Recall that the cross-covariance of variables A/A_0 and B/B_0 is given by:

$$X_{(A,B)}(\tau) = \frac{1}{2\pi} \mathcal{F}^{-1} \left(\frac{\widetilde{A(t-\tau)}}{A_0} \frac{\widetilde{B(t)}}{B_0} \right), \quad (13)$$

where $\mathcal{F}^{-1}(.)$ denotes the Inverse Fourier Transform. In the product $\frac{\widetilde{A^*}}{A_0} \frac{\widetilde{B}}{B_0}$ we can safely ignore terms of $N_i N_j^*$ when $i \neq j$, for they will not contribute to the cross-correlation due to independence of the noise sources (* here denotes complex conjugation). Consequently, the expansion of the product is always linear in the absolute values of the noise sources $|N_i|^2$. This feature is important, because it assures that the cross-covariance can be written as $\chi_{(A,B)}(\tau) = \frac{1}{2\pi} \mathcal{F}^{-1} (\sum_i f_i(\omega) |N_i|^2)$, where $f_i(\omega)$ are complex functions to be determined and the summation runs over all noise sources. Because the Inverse Fourier Transform is a linear operator, we only need to calculate the Inverse Fourier Transform of each term, $f_i(\omega) |N_i|^2$, separately. The Inverse Fourier Transform of each term is given in section 1.3.4.

1.3.2 Analytical expressions for the coefficients of variation

From the above equations (10 - 13) one can also derive the coefficient of variation of all variables. Concretely, the coefficient of variation of variable A is related to its auto-covariance at zero delay:

$$\eta_A^2 := \sigma_A^2 / A_0^2 = X_{(A,A)}(0). \quad (14)$$

For example, the coefficients of variation for ϕ_C and λ can be calculated using the Inverse Fourier transform as follows:

$$\eta_{\phi_C}^2 := \mathcal{F}_{(\tau=0)}^{-1} \left[\frac{\widetilde{\delta\phi_C}}{\phi_{0,C}} \frac{\widetilde{\delta\phi_C}}{\phi_{0,C}} \right] = \mathcal{F}_{(0)}^{-1} \left[\frac{\lambda_0^2}{\lambda_E^2 + \omega^2} (|N_{\pi_C}|^2 + |N_s|^2 + T_{MC}^2 |N_M|^2 + |N_\lambda|^2) \right]. \quad (15)$$

$$\eta_\lambda^2 = \mathcal{F}_{(\tau=0)}^{-1} \left[|N_\lambda|^2 + T_{M\lambda}^2 |N_M|^2 + \frac{2\lambda_0\lambda_E}{\lambda_E^2 + \omega^2} T_{CM}T_{M\lambda} (T_{M\lambda}T_{MC}|N_M|^2 - |N_\lambda|^2) \right] \quad (16)$$

$$+ (T_{CM}T_{M\lambda})^2 \eta_{\phi_C}^2. \quad (17)$$

(Here we have used the identity $\frac{\lambda_0}{\lambda_E+i\omega} + \frac{\lambda_0}{\lambda_E-i\omega} = \frac{2\lambda_0\lambda_E}{\lambda_E^2+\omega^2}$.) To calculate these (Inverse) Fourier Transforms we use a set of identities that can be found later in this document (Section 1.3.4, Eqs. 28-38). Here we present the results (using the notation $\beta_X^i := \beta_X + \lambda_i$, with $i = 0, E$):

$$\begin{cases} \eta_{\phi_C}^2 &= \frac{\lambda_0^2}{2\lambda_E} \left(\frac{\theta_{\pi_C}^2}{\beta_{\pi_C}\beta_{\pi_C}^E} + \frac{\theta_s^2}{\beta_s\beta_s^E} + T_{MC}^2 \frac{\theta_M^2}{\beta_M\beta_M^E} + \frac{\theta_\lambda^2}{\beta_\lambda\beta_\lambda^E} \right), \\ \eta_\lambda^2 &= \frac{\theta_\lambda^2}{2\beta_\lambda} \left(1 - \frac{2\lambda_0}{\beta_\lambda^E} T_{CM} T_{M\lambda} \right) + \frac{\theta_M^2}{2\beta_M} T_{M\lambda}^2 \left(1 + \frac{2\lambda_0}{\beta_M^E} T_{CM} T_{MC} \right) + (T_{CM} T_{M\lambda})^2 \eta_{\phi_C}^2, \\ \eta_{\pi_C}^2 &= \frac{\theta_{\pi_C}^2}{2\beta_{\pi_C}} \left(1 + \frac{2\lambda_0}{\beta_{\pi_C}^E} T_{CM} (T_R + T_{M\pi}) \right) + \frac{\theta_s^2}{2\beta_s} \left(1 + \frac{2\lambda_0}{\beta_s^E} T_{CM} (T_R + T_{M\pi}) \right) \\ &\quad + \frac{\theta_M^2}{2\beta_M} (T_R + T_{M\pi})^2 \left(1 + \frac{2\lambda_0}{\beta_M^E} T_{MC} T_{CM} \right) + T_{CM}^2 (T_R + T_{M\pi})^2 \eta_{\phi_C}^2. \end{cases} \quad (18)$$

$$\begin{cases} \eta_{\phi_Y}^2 &= \frac{\theta_{\pi_Y}^2 \lambda_0}{2\beta_{\pi_Y}\beta_{\pi_Y}^0} + \frac{\theta_s^2 \lambda_0}{2\beta_s\beta_s^0} \left(1 + T_{CM} T_{MC} \frac{\lambda_0(\beta_s + \lambda_0 + \lambda_E)}{\lambda_E\beta_s^E} \right) + \frac{\theta_M^2 \lambda_0}{2\beta_M\beta_M^0} T_{MC}^2 \left(1 + T_{CM} T_{MC} \frac{\lambda_0(\beta_M + \lambda_0 + \lambda_E)}{\lambda_E\beta_M^E} \right) \\ &\quad + \frac{\theta_\lambda^2 \lambda_0}{2\beta_\lambda\beta_\lambda^0} \left(1 + T_{CM} T_{MC} \frac{\lambda_0(\beta_\lambda + \lambda_0 + \lambda_E)}{\lambda_E\beta_\lambda^E} \right) + \frac{\theta_{\pi_C}^2 \lambda_0^2}{2\beta_{\pi_C}\beta_{\pi_C}^0} T_{CM}^2 T_{MC}^2 \frac{\lambda_0(\beta_{\pi_C} + \lambda_0 + \lambda_E)}{\beta_{\pi_C}^E \lambda_E (\lambda_0 + \lambda_E)}, \\ \eta_{\pi_Y}^2 &= \frac{\theta_{\pi_Y}^2}{2\beta_{\pi_Y}} + \frac{\theta_s^2}{2\beta_s} \left(1 + 2 \frac{\lambda_0}{\beta_s^E} T_{CM} (T_R + T_{M\pi}) \right) + \frac{\theta_M^2}{2\beta_M} (T_R + T_{M\pi})^2 \left(1 + 2 \frac{\lambda_0}{\beta_M^E} T_{CM} T_{MC} \right) + T_{CM}^2 (T_R + T_{M\pi})^2 \eta_{\phi_C}^2. \end{cases} \quad (19)$$

$$\begin{cases} \eta_{\phi_H}^2 &= \frac{\theta_{\pi_H}^2 \lambda_0}{2\beta_{\pi_H}\beta_{\pi_H}^0} + \frac{\lambda_0^3 T_{CM}^2 (T_{M\pi} - T_{M\lambda})^2}{2\lambda_E(\lambda_0 + \lambda_E)} \left(\frac{\theta_{\pi_C}^2 (\beta_{\pi_C} + \lambda_0 + \lambda_E)}{\beta_{\pi_C}\beta_{\pi_C}^0\beta_{\pi_C}^E} + \frac{\theta_s^2 (\beta_s + \lambda_0 + \lambda_E)}{\beta_s\beta_s^0\beta_s^E} \right) \\ &\quad + \frac{\theta_M^2 \lambda_0 (T_{M\pi} - T_{M\lambda})^2}{2\beta_M\beta_M^0} \left(1 + T_{CM} T_{MC} \frac{\lambda_0(\beta_M + \lambda_0 + \lambda_E)}{\lambda_E\beta_M^E} \right) \\ &\quad + \frac{\theta_\lambda^2 \lambda_0}{2\beta_\lambda\beta_\lambda^0} \left(1 + T_{CM} (T_{M\pi} - T_{M\lambda}) \frac{\lambda_0(\beta_\lambda + \lambda_0 + \lambda_E)}{\beta_\lambda^E(\lambda_0 + \lambda_E)} \left(T_{CM} (T_{M\pi} - T_{M\lambda}) \frac{\lambda_0}{\lambda_E} + 2 \right) \right) \\ \eta_{\pi_H}^2 &= \frac{\theta_{\pi_H}^2}{2\beta_{\pi_H}} + \frac{\theta_M^2}{2\beta_M} T_{M\pi}^2 \left(1 + 2 \frac{\lambda_0}{\beta_M^E} T_{CM} T_{MC} \right) + T_{CM}^2 T_{M\pi}^2 \eta_{\phi_C}^2. \end{cases} \quad (20)$$

1.3.3 Analytical expressions for the cross-covariances

Now we are in the position to present explicit expressions for the cross-covariances, which, normalised by the above variances, will result in cross-correlations: $R_{(A,B)}(\tau) = \chi_{(A,B)}(\tau) / \sqrt{\sigma_A^2 \sigma_B^2}$. The cross-covariances use functional forms A, B, S, D^1, D^2, D^3 , which are described on the next page, and the relation $A(t) + A(-t) = 2 \frac{\lambda_E}{\lambda_0} S(t)$:

$$\chi_{(\phi_C, \lambda)}(t) = T_{CM} T_{M\lambda} \left[S_{\pi_C}(t) + S_s(t) + T_{MC}^2 S_M(t) + S_\lambda(t) \right] + T_{MC} T_{M\lambda} A_M(t) - A_\lambda(t). \quad (21)$$

$$\begin{aligned} \chi_{(\pi_C, \lambda)}(t) &= T_{CM}^2 T_{M\lambda} (T_R + T_{M\pi}) \left[S_{\pi_C}(t) + S_s(t) + T_{MC}^2 S_M(t) + S_\lambda(t) \right] + (T_R + T_{M\pi}) T_{M\lambda} B_M(t) \\ &\quad + T_{CM} T_{M\lambda} \left[A_{\pi_C}(-t) + A_s(-t) \right] + \frac{2\lambda_E}{\lambda_0} T_{CM} T_{M\lambda} T_{MC} (T_R + T_{M\pi}) S_M(t) \\ &\quad - T_{CM} (T_R + T_{M\pi}) A_\lambda(t). \end{aligned} \quad (22)$$

$$\begin{aligned}\chi_{(\phi_Y, \lambda)}(t) &= T_{MC}T_{M\lambda}A_M^0(t) - A_\lambda^0(t) \\ &\quad + T_{CM}T_{M\lambda}\left[D_s^1(t) + T_{MC}^2D_M^1(t) + D_\lambda^1(t)\right] + T_{CM}T_{MC}\left[T_{MC}T_{M\lambda}D_M^2(t) - D_\lambda^2(t)\right] \\ &\quad + T_{CM}^2T_{MC}T_{M\lambda}\left[D_{\pi_C}^3(t) + D_s^3(t) + T_{MC}^2D_M^3(t) + D_\lambda^3(t)\right].\end{aligned}\tag{23}$$

$$\begin{aligned}\chi_{(\pi_Y, \lambda)}(t) &= T_{M\lambda}(T_R + T_{M\pi})B_M(t) + \frac{2\lambda_E}{\lambda_0}T_{CM}T_{MC}T_{M\lambda}(T_R + T_{M\pi})S_M(t) \\ &\quad + T_{CM}\left[T_{M\lambda}A_s^E(-t) - (T_R + T_{M\pi})A_\lambda^E(t)\right] \\ &\quad + T_{CM}^2(T_R + T_{M\pi})T_{M\lambda}\left[S_{\pi_C}(t) + S_s(t) + T_{MC}^2S_M(t) + S_\lambda(t)\right].\end{aligned}\tag{24}$$

$$\begin{aligned}\chi_{(\phi_H, \lambda)} &= (T_{M\pi} - T_{M\lambda})T_{M\lambda}A_M^0(t) - A_\lambda^0(t) + T_{CM}T_{M\lambda}\left[(T_{M\pi} - T_{M\lambda})T_{MC}D_M^1(t) + D_\lambda^1(t)\right] \\ &\quad + T_{CM}(T_{M\pi} - T_{M\lambda})\left[T_{MC}T_{M\lambda}D_M^2(t) - D_\lambda^2(t)\right] \\ &\quad + T_{CM}^2(T_{M\pi} - T_{M\lambda})T_{M\lambda}\left[D_{\pi_C}^3(t) + D_s^3(t) + T_{MC}^2D_M^3(t) + D_\lambda^3(t)\right].\end{aligned}\tag{25}$$

$$\begin{aligned}\chi_{(\pi_H, \lambda)} &= T_{M\pi}T_{M\lambda}B_M(t) + \frac{2\lambda_E}{\lambda_0}T_{M\pi}(T_{MC}T_{CM}T_{M\lambda})S_M(t) - T_{CM}T_{M\pi}A_\lambda(-t) \\ &\quad + T_{CM}^2T_{M\pi}T_{M\lambda}\left[S_{\pi_C}(t) + S_s(t) + T_{MC}^2S_M(t) + S_\lambda\right].\end{aligned}\tag{26}$$

The variances and cross-covariances presented here can be further studied and checked with the Mathematica notebook/supplementary file ‘VarianceChecker.nb’, which is available online: <https://github.com/Jintram/DynamicalRegulationBacterialCells>.

1.3.4 Functional forms of the building blocks

In the above equations, A , S , B , and D^1 , D^2 and D^3 are functional forms that will be described below. The functional forms are found by complex integration using Cauchy’s Residue theorem

and are given by:

$$A^j(t) = \int \frac{e^{i\omega t}}{2\pi} \frac{\lambda_0}{\lambda_j - i\omega} \frac{\theta^2}{\beta^2 + \omega^2} d\omega, \quad \text{for } j \in \{0, E\}, \text{ but superscript "E" is implicit} \quad (27)$$

$$= \frac{\theta^2 \lambda_0}{2\beta} \begin{cases} \frac{2\beta e^{\lambda_j t}}{\beta^2 - \lambda_j^2} - d \frac{e^{\beta t}}{\beta(\beta - \lambda_j)}, & \text{for } t < 0, \\ \frac{e^{-\beta t}}{\beta_x + \lambda_j}, & \text{for } t \geq 0. \end{cases} \quad (28)$$

$$S(t) = \int \frac{e^{i\omega t}}{2\pi} \frac{\lambda_0^2}{\lambda_E^2 + \omega^2} \frac{\theta^2}{\beta^2 + \omega^2} d\omega \quad (29)$$

$$= \frac{\theta^2 \lambda_0^2}{2(\beta^2 - \lambda_E^2)} \left(\frac{e^{-\lambda_E |t|}}{\lambda_E} - \frac{e^{-\beta |t|}}{\beta} \right) \quad (30)$$

$$D^1(t) = \int \frac{e^{i\omega t}}{2\pi} \frac{\lambda_0^2}{(\lambda_E + i\omega)(\lambda_0 - i\omega)} \frac{\theta^2}{\beta^2 + \omega^2} d\omega \quad (31)$$

$$= \theta^2 \lambda_0^2 \begin{cases} \frac{e^{\lambda_0 t}}{(\beta^2 - \lambda_0^2)(\lambda_0 + \lambda_E)} - \frac{e^{\beta t}}{2\beta \beta_x^E (\beta - \lambda_0)}, & \text{for } t < 0, \\ \frac{e^{-\lambda_E t}}{(\beta^2 - \lambda_E^2)(\lambda_0 + \lambda_E)} - \frac{e^{-\beta t}}{2\beta \beta^0 (\beta - \lambda_E)}, & \text{for } t \geq 0 \end{cases} \quad (32)$$

$$D^2(t) = \int \frac{e^{i\omega t}}{2\pi} \frac{\lambda_0^2}{(\lambda_E - i\omega)(\lambda_0 - i\omega)} \frac{\theta^2}{\beta^2 + \omega^2} d\omega \quad (33)$$

$$= \theta^2 \lambda_0^2 \begin{cases} \frac{e^{\beta t}}{2\beta(\beta - \lambda_0)(\beta - \lambda_E)} + \frac{1}{\lambda_0 - \lambda_E} \left(\frac{e^{\lambda_E t}}{\beta^2 - \lambda_E^2} - \frac{e^{\lambda_0 t}}{\beta^2 - \lambda_0^2} \right), & \text{for } t < 0, \\ \frac{e^{-\beta t}}{2\beta \beta^E \beta^0}, & \text{for } t \geq 0 \end{cases} \quad (34)$$

$$D^3(t) = \int \frac{e^{i\omega t}}{2\pi} \frac{\lambda_0^3}{(\lambda_E^2 + \omega^2)(\lambda_0 - i\omega)} \frac{\theta^2}{\beta^2 + \omega^2} d\omega \quad (35)$$

$$= \frac{\theta^2 \lambda_0^3}{2} \begin{cases} \left(\frac{e^{\beta t}}{\beta(\beta - \lambda_0)(\beta^2 - \lambda_E^2)} - \frac{2e^{\lambda_0 t}}{(\beta^2 - \lambda_0^2)(\lambda_0^2 - \lambda_E^2)} + \frac{e^{-\lambda_E t}}{\lambda_E(\beta^2 - \lambda_E^2)(\lambda_0 - \lambda_E)} \right), & \text{for } t < 0, \\ \frac{e^{-\beta t}}{\lambda_E(\lambda_0 + \lambda_E)(\beta^2 - \lambda_E^2)} - \frac{e^{-\beta t}}{\beta \beta^0 (\beta^2 - \lambda_E^2)}, & \text{for } t \geq 0 \end{cases} \quad (36)$$

$$B(t) = \int \frac{e^{i\omega t}}{2\pi} \frac{\theta^2}{\beta^2 + \omega^2} d\omega \quad (37)$$

$$= \frac{\theta^2}{2\beta} e^{-\beta |t|}. \quad (38)$$

Note that the functions D^1 and S are very similar: the only difference is a single timescale change from λ_0 to λ_E . Functions D^2 and D^3 appear only in terms representing contributions of noise that propagates a full circle, reverberating through the entire cell, starting in ϕ_C , passing through metabolism and growth, and eventually reaching the reporters.

2 Analysing the cross-correlations

The cross-correlation between two signals A and B (covariances of A and B divided by their standard deviations) contains temporal information about the dynamical interplay of the two signals. For example, if noise first reaches signal A and only later arrives at B , their cross-correlation will peak at a positive delay time. Generally, the complicated expressions for the cross-correlations between A and B indeed consists of several terms that each correspond to a different mechanism by which noise can travel from some source to A and B . Insight into these different mechanisms can be gained by splitting the mathematical description of the cross-correlation into different ‘modes’ that can each be interpreted as a different way in which noise can propagate through the cell. However, such a decomposition is not unique and hence subject to convention. Therefore, we first discuss a decomposition from Kiviet *et al.* [1] using the $\phi_C\text{-}\lambda$ cross-covariance, $\chi_{\phi_C,\lambda}$ as an example. Next, we propose a new decomposition that is better suited to the system investigated in this work.

2.1 The $\phi_C\text{-}\lambda$ cross-correlation: Old Decomposition

First, we split up the $\phi_C\text{-}\lambda$ cross-covariance (see Eq. 21) in the same way as in Kiviet *et al.*, using three modes:

- **Catabolic mode.** This mode contains the contributions of all paths that transfer via catabolism (*i.e.* from ϕ_C to M and from M to λ), where one route ends at the growth rate, and the other at protein concentration:

$$T_{CM}T_{M\lambda}(S_{\pi_C} + S_s + T_{MC}^2S_M + (-1)^2S_\lambda).$$

- **Common mode.** This mode originates from phenomenological noise source that directly influences the growth rate, and the production rates (which in turn influences the concentrations):

$$T_{MC}T_{M\lambda}A_M.$$

- **Dilution mode.** This mode represents direct transfer from growth to protein concentration:

$$-A_\lambda.$$

2.2 The $C\text{-}\lambda$ cross-correlations: New decomposition

In the current work, we argue to define the modes slightly different. The major difference is in the interpretation of the *common* mode, which is now not defined as contributions to the cross-correlations originating from a particular noise source, but rather as all contributions that are sensed commonly by all proteins in the cell. Specifically, noise in the production of particular proteins can contribute to fluctuations of M , from where it will transfer to all proteins commonly. In other words, noise that originates in a particular part of the cell can propagate through the cell and partly *become* common noise, transferring further to all proteins equally. Additionally we introduce the regulation mode, which contains all contributions to the cross-correlations that rely on the regulation and hence scale linearly with T_R .

With these conventions, the decomposition of the cross-correlation between ϕ_C and λ becomes as follows. For some terms we have added red brackets that divide the transfer parameters into specific groups of transfer parameters that are associated with a particular noise route through the cell (Figs. S1 and S2). From every noise source one can indeed follow two distinct paths, one

to each of the variables for which the cross-correlation is calculated. However, sometimes noise routes are merged for clarity of reading. Then, the red brackets are omitted.

- $\chi_{(\phi_C, \lambda)}$:

1. **Control:** $(T_{CM} T_{M\lambda}) (S_{\pi_C} + S_s)$.
2. **Dilution:** $-A_\lambda$.
3. **Common:** $(T_{M\pi} - T_{M\lambda}) T_{M\lambda} A_M + (T_{CM} T_{M\lambda}) \left[T_{MC}^2 S_M + (-1)^2 S_\lambda \right]$.
4. **Regulation:** $T_R T_{M\lambda} A_M$.

- $\chi_{(\pi_C, \lambda)}$:

1. **Control:** $(T_{CM} T_{M\lambda}) (A_{\pi_C}(-t) + A_s(-t))$.
2. **Dilution:** 0.
3. **Common:** $T_{M\pi} T_{M\lambda} B_M + (T_{CM} T_{M\pi}) (T_{CM} T_{M\lambda}) \left[(S_{\pi_C} + S_s + T_{MC}^2 S_M + (-1)^2 S_\lambda) + 2 \frac{\lambda_E}{\lambda_0} T_{MC} T_{CM} T_{M\pi} T_{M\lambda} S_M - (T_{CM} T_{M\pi}) A_\lambda \right]$.
4. **Regulation:** $T_R T_{M\lambda} B_M + (T_{CM} T_R) (T_{CM} T_{M\lambda}) \left[S_{\pi_C} + S_s + T_{MC}^2 S_M + S_\lambda \right] + 2 \frac{\lambda_E}{\lambda_0} T_{MC} T_{CM} T_R T_{M\lambda} S_M - (T_{CM} T_R) A_\lambda$.

The above equations for $\chi_{(\phi_C, \lambda)}$ and $\chi_{(\pi_C, \lambda)}$ apply to both wild type *E. coli* cells and the cAMP-fixed *cyaA cpdA* null mutant studied in the main text. This allows us to pinpoint the role of regulation in shaping the cross-correlation. The parameter T_R that represents the cAMP-CRP regulation feedback is expected to be negative in the wild type ($T_R < 0$ due to cAMP-CRP regulation). In the cAMP-fixed strain however, the negative feedback is abolished and $T_R = 0$. Such a parametric switch will qualitatively change the cross-correlations $R_{(\phi_C, \lambda)}$ and $R_{(\pi_C, \lambda)}$. For example, a negative contribution with functional form of A_M (asymmetrically, left-skewed function with timescale λ_0) is effectively removed from $R_{(\phi_C, \lambda)}$.

Note that T_R however not only influences the presence and absence of modes. Additionally, T_R also influences the coefficients of variation (Eqs. 18 - 20), and amplitudes and timescales of the other modes via $\lambda_E := \lambda_0(1 - (T_R + T_{M\pi} - T_{M\lambda}))$. Most modes are therefore expected to show slight, quantitative differences between wild type and cAMP-fixed cells, but only the regulation mode will show a strong qualitative difference: it is completely absent in cAMP-fixed cells.

2.3 Summary of the new decomposition for the reporters

2.3.1 $\chi(\phi_Y, \lambda)$

1. **Control:** $(T_{CM} T_{M\lambda}) D_s^1$.
2. **Dilution:** $-A_\lambda^0$.
3. **Common:** $(T_{M\pi} - T_{M\lambda}) T_{M\lambda} A_M^0 + T_{CM} T_{MC} (T_{MC} T_{M\lambda} D_M^2 - D_\lambda^2) + (T_{CM} (T_{M\pi} - T_{M\lambda})) (T_{CM} T_{M\lambda}) \left[D_{\pi_C}^3 + D_s^3 + T_{MC}^2 D_M^3 + D_\lambda^3 \right] + (T_{MC} T_{CM} (T_{M\pi} - T_{M\lambda})) T_{M\lambda} D_M^1 + (T_{CM} T_{M\lambda}) D_\lambda^1$.
4. **Regulation:** $T_R T_{M\lambda} A_M^0 + (T_{CM} T_R) (T_{CM} T_{M\lambda}) \left[D_{\pi_C}^3 + D_s^3 + T_{MC}^2 D_M^3 + D_\lambda^3 \right] + (T_{MC} T_{CM} T_R) T_{M\lambda} D_M^1$.

2.3.2 $\chi(\pi_Y, \lambda)$

1. **Control:** $(T_{CM}T_{M\lambda}) A_s(-t)$.
2. **Dilution:** 0.
3. **Common:** $T_{M\pi}T_{M\lambda}B_M + (T_{CM}T_{M\pi}) (T_{CM}T_{M\lambda}) \left[S_{\pi_C} + S_s + T_{MC}^2 S_M + S_\lambda \right] + 2\frac{\lambda_E}{\lambda_0} T_{M\pi} (T_{MC}T_{CM}T_{M\lambda}) S_M - (T_{CM}T_{M\pi}) A_\lambda$.
4. **Regulation:** $T_R T_{M\lambda} B_M + (T_{CM}T_R) (T_{CM}T_{M\lambda}) \left[S_{\pi_C} + S_s + T_{MC}^2 S_M + S_\lambda \right] + 2\frac{\lambda_E}{\lambda_0} T_R (T_{MC}T_{CM}T_{M\lambda}) S_M - (T_{CM}T_R) A_\lambda$.

2.3.3 $\chi(\phi_H, \lambda)$

1. **Control:** 0.
2. **Dilution:** $-A_\lambda^0$.
3. **Common:** $(T_{M\pi} - T_{M\lambda}) T_{M\lambda} A_M^0 + T_{CM} T_{MC} (T_{MC} T_{M\lambda} D_M^2 - D_\lambda^2) + (T_{CM} (T_{M\pi} - T_{M\lambda})) (T_{CM} T_{M\lambda}) \left[D_{\pi_C}^3 + D_s^3 + T_{MC}^2 D_M^3 + D_\lambda^3 \right] + (T_{MC} T_{CM} (T_{M\pi} - T_{M\lambda})) T_{M\lambda} D_M^1 + (T_{CM} T_{M\lambda}) D_\lambda^1$.
4. **Regulation:** 0.

2.3.4 $\chi(\pi_H, \lambda)$

1. **Control:** 0.
2. **Dilution:** 0.
3. **Common:** $T_{M\pi}T_{M\lambda}B_M + (T_{CM}T_{M\pi}) (T_{CM}T_{M\lambda}) \left[S_{\pi_C} + S_s + T_{MC}^2 S_M + S_\lambda \right] + 2\frac{\lambda_E}{\lambda_0} T_{M\pi} (T_{MC}T_{CM}T_{M\lambda}) S_M - (T_{CM}T_{M\pi}) A_\lambda$.
4. **Regulation:** 0.

2.4 Example: interpretation of the decomposition of the $\phi_Y - \lambda$ cross-correlations

To clarify the interpretation of the expressions above, we now discuss the decomposition of the $Y-\lambda$ cross-correlation function in detail.

1. **Catabolism mode.** This mode is a consequence of fluctuations in the expression level of the catabolic sector (C-sector) that directly influence the rate of metabolism and the growth rate. Even though the reporter Y is itself not metabolically active, it does share a noise source (N_s) with the C-sector. As a result, the (cross-)correlation $R_{(\phi_Y, \lambda)}$ also contains the catabolism mode, reflecting that ϕ_Y correlates with ϕ_C (due to the shared noise source N_s), and ϕ_C with λ (due to the effect that fluctuations in ϕ_C have on the growth rate).

$$T_{CM} T_{M\lambda} D_s^1.$$

Note that indeed only the shared noise source N_s transfers directly to growth from π_Y , instead of reverberating through metabolism (and thus becoming ‘common’ noise). The function D^1 appears (instead of the function S as found in [1]) because noise transferring from metabolism, via production to the reporters (Y or H) has a delay timescale of λ_0 , whereas noise transferring to ϕ_C has timescale λ_E . The logic behind $D^1 - D^3$ is that: (D^1) noise transfers once via ϕ_C and once directly to ϕ_Y , obtaining timescales λ_E and λ_0 , respectively, (D^2) one route is instantaneous, but the other makes a “double” loop, affecting first ϕ_C and picking up timescale λ_E and then transferring to ϕ_Y , picking up timescale λ_0 , (D^3) appears when one route has timescale λ_E and the other route is ‘double’, picking up both λ_E and λ_0 timescales. For example, compare the two terms that originate at noise source N_M in the second line of Eq. 21. The first one can be written as $(T_{MC})(T_{MCT_{CM}T_{M\lambda}})D_M^1$ and has time scales λ_E for the route that transfers via metabolism and λ_0 for the route that goes from metabolism to ϕ_Y with parameter T_{MC} (Fig. S2A). The other term can be written as $(T_{MCT_{CM}T_{MC}})(T_{M\lambda})D_M^2$, and here one path is instantaneous ($T_{M\lambda}$) and the other transfers first from M to ϕ_C with timescale λ_E and afterwards to ϕ_Y with timescale λ_0 (Fig. S2B).

2. **Dilution mode.** This represents direct transfer from growth to protein concentration.

$$-A_\lambda^0.$$

3. **Common mode.**

$$(T_{M\pi} - T_{M\lambda})T_{M\lambda}A_M^0 + T_{CM}T_{MC}(T_{MCT_{M\lambda}}D_M^2 - D_\lambda^2) + (T_{CM}(T_{M\pi} - T_{M\lambda})) (T_{CM}T_{M\lambda}) \left[D_{\pi_C}^3 \right. \\ \left. + D_s^3 + T_{MC}^2 D_M^3 + D_\lambda^3 \right] + (T_{MCT_{CM}}(T_{M\pi} - T_{M\lambda})) T_{M\lambda}D_M^1 + (T_{CM}T_{M\lambda}) D_\lambda^1.$$

Common noise now also includes noise in the C -sector, and its effect on the reporters after it reverberated through the cell. Here, one can for example examine the term $(-T_{CM}T_{M\lambda})(-T_{CM}(T_{M\pi} - T_{M\lambda}))D_\lambda^3$, where both the path that ends up in λ , $(-T_{CM}T_{M\lambda})$, as well as the path that end up in ϕ_Y , $(-T_{CM}(T_{M\pi} - T_{M\lambda}))$ make a route where it crosses ϕ_C , picking up a timescale of λ_E and after that one route transfers to ϕ_Y , picking up a timescale λ_0 . Another interesting example is the second term, $-T_{CM}(T_{M\pi} - T_{M\lambda})D_\lambda^2$, this is growth-noise that diluted ϕ_C , which has affected metabolism, but from there transfers equally to all other proteins (with coefficient $T_{M\pi} - T_{M\lambda}$). Therefore, this term is now also regarded as common noise.

4. **Regulation**

$$T_R T_{M\lambda} A_M^0 + (T_{CM}T_R) (T_{CM}T_{M\lambda}) \left[D_{\pi_C}^3 + D_s^3 + T_{MC}^2 D_M^3 + D_\lambda^3 \right] + (T_{MCT_{CM}T_R}) T_{M\lambda} D_M^1.$$

In the decompositions we often have the term $T_{M\pi} - T_{M\lambda}$. This represents the net transfer from M to ϕ via π and from M to ϕ via λ . Red brackets can help to identify the noise route.

3 Parameter reduction

In this section, we show that two parameters can be effectively scaled away from the system, resulting in fewer parameters to be fitted. First of all, since cross-correlations are dimensionless

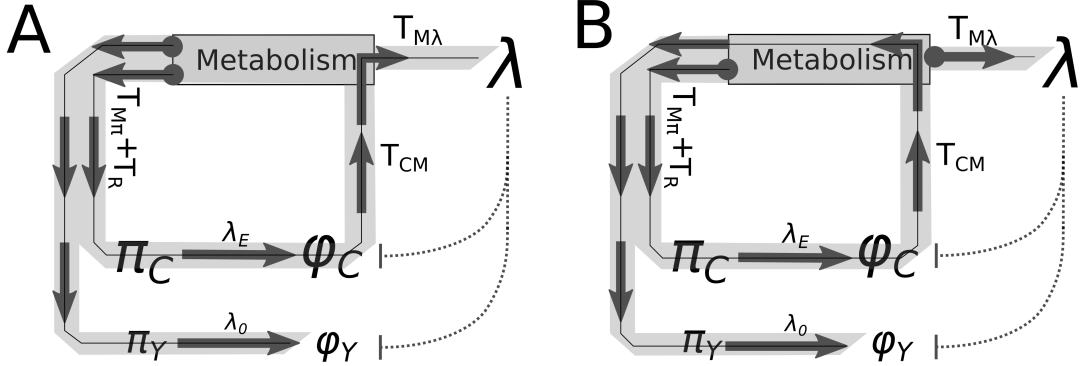


Figure S2: Example analysis of the noise routes (shown here is a part of the network.) (A) Example of a M -noise route that appears in the $\phi_Y - \lambda$ cross-correlation. Transfer coefficients can be split up to represent the paths to ϕ_C and to λ separately as: (T_{MC}) $(T_{MC}T_{CM}T_{M\lambda})$. (B) Another example of a M -noise route: $(T_{MC}T_{CM}T_{MC})$ $(T_{M\lambda})$.

measures, we can set one noise amplitude to 1. We pick θ_s , since this noise source has to be present to find any difference between the two reporters in cAMP-fixed cells. Second, note that we do not measure M , so that we can scale away T_{CM} , and consider fluctuations in $\delta M / (T_{CM}M_0)$ with scaled noise source $N'_M = N_M / T_{CM}$.

Now, to do the parameter reductions formally, we start with the original system (Eqs. 1-8):

$$\frac{\delta \lambda}{\lambda_0} = N_\lambda + T_{M\lambda} \frac{\delta M}{M_0}, \quad (39)$$

$$\frac{\delta M}{M_0} = N_M + T_{CM} \frac{\delta \phi_C}{\phi_{C,0}} = T_{CM} \left(\frac{N_M}{T_{CM}} + \frac{\delta \phi_C}{\phi_{C,0}} \right), \quad (40)$$

$$\frac{\delta \pi_C}{\pi_{0,C}} = N_{\pi_C} + N_s + (T_{M\pi} + T_R) \frac{\delta M}{M_0}, \quad (41)$$

$$\frac{\delta \pi_y}{\pi_{0,y}} = N_{\pi_Y} + N_s + (T_{M\pi} + T_R) \frac{\delta M}{M_0}, \quad (42)$$

$$\frac{\delta \pi_H}{\pi_{0,H}} = N_{\pi_H} + T_{M\pi} \frac{\delta M}{M_0}. \quad (43)$$

Defining $\hat{\delta M} = \frac{\delta M}{T_{CM}M_0}$, $\hat{N}_M = N_M / T_{CM}$, $\hat{T}_{M\lambda} = T_{CM}T_{M\lambda}$, $\hat{T}_{M\pi} = T_{CM}T_{M\pi}$ and $\hat{T}_R = T_{CM}T_R$ This

system can then be transformed to:

$$\frac{\delta\lambda}{\lambda_0} = N_\lambda + T_{M\lambda} \left(T_{CM} \delta \hat{M} \right) = N_\lambda + T_{M\lambda} \delta \hat{M}, \quad (44)$$

$$\delta \hat{M} = \hat{N}_M + \frac{\delta \phi_C}{\phi_{C,0}} \quad (45)$$

$$\frac{\delta \pi_C}{\pi_{0,C}} = N_{\pi_C} + N_s + (T_{M\pi} + T_R) \left(T_{CM} \delta \hat{M} \right) = N_{\pi_C} + N_s + (T_{M\pi} + T_R) \delta \hat{M}, \quad (46)$$

$$\frac{\delta \pi_Y}{\pi_{0,Y}} = N_{\pi_Y} + N_s + (T_{M\pi} + T_R) \left(T_{CM} \delta \hat{M} \right) = N_{\pi_Y} + N_s + (T_{M\pi} + T_R) \delta \hat{M}, \quad (47)$$

$$\frac{\delta \pi_H}{\pi_{0,H}} = N_{\pi_H} + T_{M\pi} \left(T_{CM} \delta \hat{M} \right) = N_{\pi_H} + T_{M\pi} \delta \hat{M}. \quad (48)$$

Next, we divide all noise sources by θ_s , since all cross-covariances and all variances are linear in terms of θ_i^2 (the noise amplitude of each independent noise source i). Thus, if we scale all noise sources with θ_s , the resulting cross-correlations (cross-covariances divided by variance) do not change. How the parameter reduction, and the scaling by θ_s affects the functional form of the cross-correlation between signals A and B is shown below, where we split the cross-covariance and the variances in contributions of each noise source. We explicitly write the contribution of noise source N_M , associated with noise amplitude θ_M and only later replace its parameters with $\hat{\theta}_M := \theta_M/T_{CM}$. The contribution of each noise source i to the cross-covariance is written as f_i (time dependence is omitted for readability) and we write g_A and h_B for the noise source's contribution to the variance of A and B respectively. Then:

$$R_{(A,B)}(\tau) = \frac{\left(\frac{\theta_M}{T_{CM}} \right)^2 f_M + \sum_{i \neq M} \theta_i^2 f_i(\tau)}{\sqrt{\left(\frac{\theta_M}{T_{CM}} \right)^2 g_{A,M}(\tau) + \sum_{i \neq M} \theta_i^2 g_{A,i}} \sqrt{\left(\frac{\theta_M}{T_{CM}} \right)^2 h_{B,M} + \sum_{i \neq M} \theta_i^2 h_{B,i}}} \quad (49)$$

$$= \frac{\left(\frac{\theta_M/\theta_s}{T_{CM}} \right)^2 f_M + f_s + \sum_{i \neq s,M} (\theta_i/\theta_s)^2 f_i}{\sqrt{\left(\frac{\theta_M/\theta_s}{T_{CM}} \right)^2 g_{A,M} + g_{A,s} + \sum_{i \neq s,M} (\theta_i/\theta_s)^2 g_{A,i}} \sqrt{\left(\frac{\theta_M/\theta_s}{T_{CM}} \right)^2 h_{B,M} + h_{B,s} + \sum_{i \neq s,M} (\theta_i/\theta_s)^2 h_{B,i}}} \quad (50)$$

$$= \frac{\left(\hat{\theta}_M \right)^2 f_M + f_s + \sum_{i \neq s,M} \hat{\theta}_i^2 f_i}{\sqrt{\left(\hat{\theta}_M \right)^2 g_{A,M} + g_{A,s} + \sum_{i \neq s,M} \hat{\theta}_i^2 g_{A,i}} \sqrt{\left(\hat{\theta}_M \right)^2 h_{B,M} + h_{B,s} + \sum_{i \neq s,M} \hat{\theta}_i^2 h_{B,i}}}. \quad (51)$$

Here, $\hat{\theta}_i = \theta_i/\theta_s$, and $\hat{\theta}_M = \frac{\theta_M/\theta_s}{T_{CM}}$. By considering only $\hat{\cdot}$ -parameters, we effectively removed two parameters from the model.

4 Data analysis

4.1 Calculating cross-correlations from data

Segmentation was done using the software Schnitzcells, developed by the Elowitz lab [3], with custom scripts written by Daan Kiviet, Philippe Nghe and Noreen Walker. Tracking was done in line with Kiviet *et al* [1]. Cell length is used by fitting a 3rd (or, in some cases 5th) order polynomial through the cell area. Cross-covariance S and cross-correlation, R , between two signals in discrete time is then defined as:

$$S_{f,g}(\tau) = \frac{1}{N-1} \sum_{n=0}^{N-|\tau|-1} \hat{f}(n)\hat{g}(n+\tau). \quad (52)$$

$$R_{f,g}(\tau) = \frac{S_{f,g}(\tau)}{\sqrt{S_{f,f}(0)S_{g,g}(0)}}. \quad (53)$$

Here, hats indicate mean-subtracted signals.

Cells that are born earlier in the experiments appear in more lineages. When calculating cross-correlations along lineages, we must thus be careful to not count such cells repeatedly. Therefore, we introduce for each data point a weight, representing in how many branches the point occurs. The resulting cross-correlation is a composite cross-correlation with contributions of points from multiple branches i . Lastly, we also introduce time-average-subtracted variable, since averages can change slightly during experiments. We therefore define a composite cross-covariance and cross-correlation:

$$S_{f,g}(\tau) := \frac{1}{W_{\text{total},\tau}} \sum_i \frac{1}{N_i - |\tau|} \sum_{n=0}^{N_i - |\tau|} w_{n,i,\tau} \hat{f}_i(n) \hat{g}_i(n+\tau), \quad (54)$$

$$\mathcal{R}_{f,g}(\tau) = \frac{S_{f,g}(\tau)}{\sqrt{S_{f,f}(0)S_{g,g}(0)}}, \quad (55)$$

$$\hat{f}_i(n) = f_i(n) - \langle f_i \rangle_n \quad (56)$$

$$w_{n,i,\tau} = 1/K_{n,i,\tau}, \quad (57)$$

$$W_{\text{total},\tau} = \sum_{n,i} w_{n,i,\tau}. \quad (58)$$

Here, the summations run are over all branches i and time points n . Weights are indicated with w , where $K_{n,i,\tau}$ is the total number a specific point pair $\{\hat{f}_i(n)\}\hat{g}_i(n+\tau)$ was used. Throughout the manuscript we refer to the composite cross-correlation \mathcal{R} as the cross-correlation R . The mean-subtracted signal $\{\hat{f}_i(n)\}$ is now recalculated in each branch, for each time point to compensate for a changing overall average during the experiment.

4.2 Averaging multiple experiments and estimating error bars

The cross-correlations calculated per microcolony are averaged to create the figures 2-3. Here, we explain how we averaged the multiple (independent) experiments (each microcolony being an experiment) and how we calculated error bars. We use a Mixed Model Estimate, assuming that each individual measurement $y_{i,j}$ from experiment i is determined by the average of interest, $\langle y \rangle$, plus two noise sources: within experimental noise $\xi_i(i)$, and between-experiments noise ξ_i :

$$y_{i,j} = \langle y \rangle + \xi_i + \xi_j(i).$$

Here, ξ_i is the noise that determines the off-set of the mean from experiment i , and $\xi_j(i)$ the noise on individual measurement j in group i . Assume: $\mathbb{E}[\xi_i] = \mathbb{E}[\xi_j] = 0$ and $\text{Var}(\xi_i) = s_i^2$, the variance within experiment i , which might differ between experiments, and $\text{Var}(\xi_i) = s_\mu^2$, the variance between the means of each experiment. The within experiment variance is estimated by dividing each microcolony into four lineages (from the moment there were four cells in the microcolony, we followed each of their lineages separately), and calculating and comparing statistics along each lineage. With these notions for ξ_i and $\xi_j(i)$, we write n for the number of experiments and n_i for the number of subgroups within experiment i . Then:

$$\mathbb{E}[y_{i,j}] = \langle y \rangle \quad (59)$$

$$\text{Var}(\mathbb{E}[y_{i,j}]) = \frac{\text{Var}\left(\sum_i \sum_j \langle y \rangle + \xi_i + \xi_j(i)\right)}{(\sum_i n_i)^2} \quad (60)$$

$$= \frac{1}{(\sum_i n_i)^2} \text{Var}\left(\sum_i n_i \xi_i + \sum_i \sum_j \xi_j\right) \quad (61)$$

$$= \frac{1}{(\sum_i n_i)^2} \left(\sum_i n_i^2 \text{Var}(\xi_i) + \sum_i n_i \text{Var}(\xi_j) \right) \quad (62)$$

$$= \frac{s_\mu^2 \sum_i n_i^2 + \sum_i n_i s_i^2}{(\sum_i n_i)^2} \quad (63)$$

To calculate $\langle y \rangle$, we again use knowledge of within-experiment variances to calculate the weight factor of each microcolony: let $y_i(t)$ be the measured mean value in experiment i at time t , with within-experiments error $s_i(t)$. Then:

$$\langle y(t) \rangle = \frac{\sum_i^n s_i^{-2}(t) y_i(t)}{\sum_j^n s_j^{-2}(t)} =: \frac{\sum_i w_i(t) y_i(t)}{W(t)}.$$

Here, $w_i(t) = \frac{1}{s_i^2(t)}$ and $W(t) = \sum_{j=1}^n w_i(t)$. That is, more precise measurements (that is, those with smaller within-experiment error s_i) obtain a higher weight.

4.3 Null-expectation for the cross-correlations

To confirm that the measured cross-correlations correspond to real, biological, signals inside the cells, we performed a permutation analysis on the time-series data. We kept the temporal information of the data, but randomised at each time point the growth rate and expression data for all the cells in the colony. Any biological correlations between variables should therewith be removed. Repeating this randomisation 50 times, and each time re-calculating cross-correlations, indeed gives a band of cross-correlations around zero, allowing us to infer what kind of signals could still be explained purely by technical noise (See for example Fig. S9). Any part of the originally measured cross-correlations that fall outside this band can then be concluded to stem from a real biological signal.

Parameter	Confined to	Best Fit	95% Confidence Interval
θ_{π_C}	0	-	-
θ_s	1	-	-
T_{CM}	1	-	-
T_R	$[-2, 2]; 0$	-1.67	[-2.28,-1.25]
$\hat{T}_{M,\lambda}$	$[-1, 1]$	0.05	[0.045, 0.54]
$\hat{T}_{M,\pi}$	$[-1, 1]$	-0.179	[-0.22, -0.14]
$\hat{\theta}_{\pi_Y}$	$[0, 5]$	0.0	[0,0.74]
$\hat{\theta}_{\pi_h}$	$[0, 5]$	1.14	[1.06,1.24]
$\hat{\theta}_M$	$[0, 10]$	0.90	[0.83,0.97]
$\hat{\theta}_\lambda$	$[0, 5]$	0.13	[0.125,0.143]
β_π	> 2	2	[1.8, 2.16]
β_μ	> 0.5	0.78	[0.75,0.82]

Table S1: Best fit parameters of the wild type and optimal mutant, including predefined parameter constraints and best-fit confidence ranges based on statistical analysis. For the precise interpretation of $\hat{\cdot}$ -parameters, see section ‘Parameter Reduction’.

5 Fitting procedure

5.1 Wild type and cAMP-fixed* cells

The full mathematical model, with the reduced number of parameters, was fitted to the cross-correlations with their error bars using a weighted least-square fitting procure in Mathematica. We fitted $R_{(\phi,\lambda)}$ and $R_{(\pi,\lambda)}$ for both reporters and for wild type and cAMP-fixed* cells simultaneously.

In all fits, we set $\theta_{\pi_C} = 0$, for three reasons. First, the variable ϕ_C represents the entire C-sector, so that random, intrinsic fluctuations in the total size of this sector are expected to be small. Second, any noise source that directly influences the total size of the C-sector should also affect the CRP-reporter Y, because C and Y are regulated and expressed similarly. Such noise sources are therefore also captured by the phenomenological noise source N_s that summarises shared noise sources between the C-sector and Y. Third, fluctuations in the concentrations of each of the individual proteins of the C-sector likely transfer differently to metabolism than joined fluctuations of the entire C-sector. The effect of the intrinsic fluctuations of individual C-sector protein species on the metabolic flux is instead captured by the noise source N_M . Fluctuation in any individual C-sector protein could indeed potentially influence the flux catalysed by the entire C-sector, causing fluctuations in metabolism.

For cAMP-fixed* cells we predefined that $T_R = 0$, and for wild type cells $T_R < 0$. All other parameters were not allowed to differ between WT and cAMP-fixed* cells. We thus fitted 9 free parameters: $\{T_R \text{ (only for WT cells)}, T_{M,\lambda}, T_{M,\pi}, \theta_{\pi_Y}, \theta_{\pi_h}, \hat{\theta}_M, \hat{\theta}_\lambda, \frac{\beta_\pi}{\lambda_0}, \frac{\beta_\mu}{\lambda_0}\}$. (The hat-parameters are defined in the section ‘Parameter Reduction’, section 3; T_{CM} and θ_s , are set to unity and removed from the model by scaling.) The timescale β_π is the time-scale of the production noise rates, and β_μ is the timescale of growth/dilution-related noise sources ($\theta_s, \theta_M, \theta_\lambda$), their value given is relative to the mean growth rate, λ_0 .

In table S1 we present best-fit parameters, with their 95% confidence interval.

The 95% confidence ranges of the parameters were estimated by changing that parameter until the increase in (weighted) sum of squared residuals was statistically significant (as determined

using F-statistics).

Although the model is able to reproduce the experimentally observed cross-correlations, we are hesitant to over-interpret the exact numerical values of the fitted parameters. For example, the wild type and optimal mutant's best-fit-parameter for the transfer from M to π , $T_{M\pi}^*$, is small, but negative (Table S1). Such a negative parameter is counter-intuitive, for it results in a negative common mode (fluctuations in metabolism increase the growth rate, but lower the production rates). Presence of this negative common mode is only reflected in the mutant's negative π_H - λ cross-correlation, and, importantly, it is also this negative cross-correlation that causes the best-fit parameter to become negative (not including $R_{(\pi_H, \lambda)}$ causes the best-fit value for $T_{M\pi}^*$ to be slightly positive, data not shown). Extensions of the model with alternative mechanistic explanations that could explain the negative correlation between π_H and λ (such as competition for ribosomes at the single-cell level, or a negative control from the reporters) did also not fit the negative cross-correlation well (data not shown, Mathematica notebooks available upon request with the authors). Possibly, this specific negative cross-correlation could be caused by an experimental artefact that heavily influences the fitted parameters. Indeed, similar constitutive reporters measured in earlier work [1, 4] show a positive correlation between π_H and λ .

The model can predict preliminary coefficients of variation for the wild type and mutant cells, gaining some preliminary insight in whether cAMP-CRP feedback potentially plays the role of quenching noise. Filling the parameters from Table S1 into Equations 15 and 16, we find:

$$\eta_{\phi_C, \text{WT}}^2 / \eta_{\phi_C, \text{cAMP-fixed*}}^2 = 0.85, \quad (64)$$

$$\eta_{\lambda, \text{WT}}^2 / \eta_{\lambda, \text{cAMP-fixed*}}^2 = 0.92. \quad (65)$$

However, for the reported noise amplitudes in table S1 the absolute values for the CVs do not both seem realistic, *i.e.*, $\eta_{\phi_C, \text{WT}}^2 \approx 0.3$ and $\eta_{\lambda, \text{WT}}^2 = 0.014$. Still, this analysis might suggest a role for the cAMP-CRP mechanism to quench noise.

From the best-fit parameters above (Table S1), we qualitatively reproduced the Low cAMP cross-correlations by changing the transfer parameters to $\{T_R = 0, T_{M\lambda}^* = 0.6, T_{M\pi}^* = 0.45\}$. The timescales of each noise source relative to the growth rate (which is lower under this condition than under optimal cAMP levels) were kept constant. Although the resulting cross-correlations reproduce many qualitative features of the measurements, the mathematical model over-estimates the overall amplitude of the cross-correlation (Fig. S6A). This could perhaps be explained by experimental error: Independent measurement noise in any two variables reduces their correlation. In the model, such decorrelation can be mimicked by increasing the noise levels of θ_{π_Y} and θ_{π_H} to $\{5, 3.5\}$ respectively. An increase in those noise parameters does not affect the shape of the cross-correlation, but only decreases the overall amplitude of the cross-correlation (decorrelation).

The cross-correlation between ϕ_C and λ in the high-cAMP regime is hypothesised in the main text to posses a negative catabolism mode. When ϕ_C is over-expressed, the metabolic flux might still increase very slightly with an upward fluctuation of ϕ_C . However, the flux *per invested protein* will decrease. Since π and λ are relative quantities (both scaled with total protein mass), the negative control of ϕ_C effectively results in negative transfer from M to λ and from M to π .

Setting $\{T_R = 0, T_{M\lambda}^* = -0.8, T_{M\pi}^* = -0.47\}$ while keeping all other parameters as in Table S1) indeed qualitatively explained many features of the measured cross-correlations (Fig. S6B). However, relative to the mean growth rate, the experimentally measured cross-correlations decay faster than in the other conditions. Additionally, the high-cAMP cross-correlations are again over-estimated by the model. Another clear mismatch is that, for these parameters, the model predicts a strong common mode (which can be seen most clearly in the π_H - λ cross-correlation) that does not seem to be present in the data (although, one microcolony did show a clear positive

π_H - λ cross-correlation, see bottom right panel in Fig. S7). Interestingly, just as in the wild type, the cross-correlations of both reporter look similar in cAMP-fixed cells under the high-cAMP condition. Possibly, the noise amplitude of the CRP protein (N_s) is lower under this condition, such that the C-sector reporter is less correlated with the C-sector and behaves more similar to the constitutive reporter. A semi-quantitative fit can made (see also Fig. 3 of the main text) by further tuning: $\{\hat{T}_{M\lambda} = -0.6, \hat{T}_{M\pi} = -0.25, \hat{\theta}_{\pi_Y} = 2.5, \hat{\theta}_{\pi_h} = 4, \hat{\theta}_M = 1.8, \hat{\theta}_\lambda = 0.8, \beta_\pi = 2\lambda_0, \beta_\mu = 1.2\lambda_0\}$. This correspond with a decrease in θ_s of roughly a factor 2, and with a slight increase in θ_λ , also roughly a factor 2.

6 Toy model of the means of the two reporters

From the observation that the sum of the concentration of both reporters is, on average (Fig. S10A), approximately constant, we were inspired to also write equations for the population-level average behaviour. We here derive a phenomenological toy model that describes how the average concentrations, production rates and growth rates of cAMP-fixed cells change under changing external cAMP concentration.

Generally, we can write for the (average) total concentration of the catabolic sector ϕ_C and for the constitutive reporter H :

$$\frac{\partial \phi_C}{\partial t} = \pi_C - \phi_C \lambda = (f_C(x) - \phi_C) \lambda, \quad (66)$$

$$\frac{\partial \phi_H}{\partial t} = \pi_H - \phi_H \lambda = (f_H - \phi_H) \lambda. \quad (67)$$

Here $f_C(x)$ is a regulation function that determines the fraction of all metabolic flux allocated towards production of ϕ_C as a function of some internal metabolite (in this case, x reflect the internal cAMP concentration). However, f_H is also not necessarily a constant and can depend on resource allocation. We will show below that f_H is indeed not constant.

From the experiments we observe $\phi_Y + \phi_H$ is approximately a constant. Assuming that Y is a good reporter of the C sector, this is equivalent to:

$$\phi_C + \phi_H = T$$

(Note that this ignores proteomic shifts that result from a changing the ribosomal sector, or any other sector that is not modelled here.) In the steady state, $\phi_H = f_H$, and therefore also $\pi_H = \phi_H \lambda = (T - f_C(x)) \lambda = f_H \lambda$. We can thus rewrite the differential equation for H as:

$$\frac{\partial \phi_H}{\partial t} = (T - f_C(x)) \lambda - \phi_H \lambda.$$

In steady state, this suggest that the production rates (as directly quantified from the experiments), divided by the growth rates should be equal to the concentration for both the reporters (Fig. S10A).

In the mutant, the growth rate declines when either over, or under-expressing ϕ_C , and the mean growth rates fit a 2nd order polynomial nicely.

$$\lambda(\phi_C) := g_\lambda(\phi_Y) = a\phi_Y^2 + b\phi_Y + c$$

For best-fit parameters $\{a = -3.94 \cdot 10^{-5}, b = 2.12 \cdot 10^{-2}, c = -2.02\}$. Here we consider ϕ_C , the metabolic sector, well-reported by the metabolic reporter ϕ_Y .

Using this polynomial, the relationships between mean protein production rates/mean protein concentrations, and the mean growth rate can be related (Figs. S3 and S10):

$$\{\phi_Y, \lambda\} = \{\phi_Y, g_\lambda(\phi_Y)\}, \quad (68)$$

$$\{\pi_Y, \lambda\} = \{\phi_Y g_\lambda(\phi_Y), g_\lambda(\phi_Y)\}, \quad (69)$$

$$\{\phi_H, \lambda\} = \{\phi_H, g_\lambda(T - \phi_H)\}, \quad (70)$$

$$\{\pi_H, \lambda\} = \{\phi_H g_\lambda(T - \phi_H), g_\lambda(1 - \phi_H)\}, \quad (71)$$

$$\{\pi_Y, \pi_H\} = \{\phi_Y g_\lambda(T - \phi_H), \phi_H g_\lambda(T - \phi_H)\}. \quad (72)$$

These relationships fit strikingly well (Fig. S10).

7 Supplementary Figures

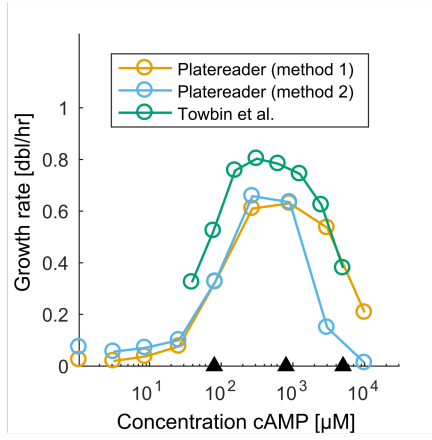


Figure S3: Growth rates in minimal medium supplemented with lactose and various cAMP concentrations. Measured exponential phase growth rates of the *cyaA cpdA* null mutant (cAMP-fixed cells) at different concentrations of cAMP as measured in a plate reader. Black triangles refer to the low, optimal and high cAMP concentrations respectively. Method 1 refers to a procedure where the growth rate was determined as an exponential fit over a manually selected part of the bacterial density curve, whereas in method 2 we fitted an exponential to the part of the bacterial density curve that fell between two threshold values. Additionally, this figure shows data from a similar experiments performed by Towbin *et al.* [5]

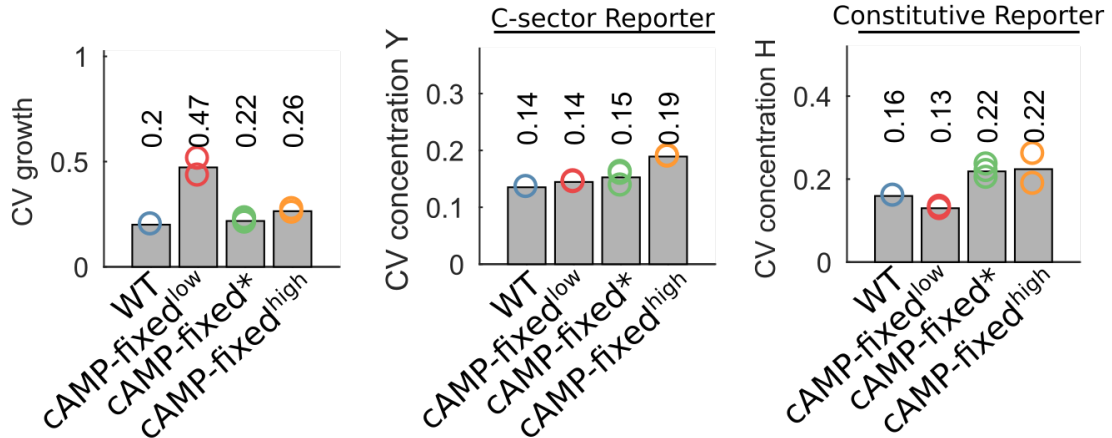


Figure S4: Coefficients of variation of the growth rate (left panel) and the concentrations of the C-sector reporter (middle panel) and the constitutive reporter (right panel) for the different conditions. Shown in the figure are only the experiments performed with a similar microscope such that their absolute values were comparable.

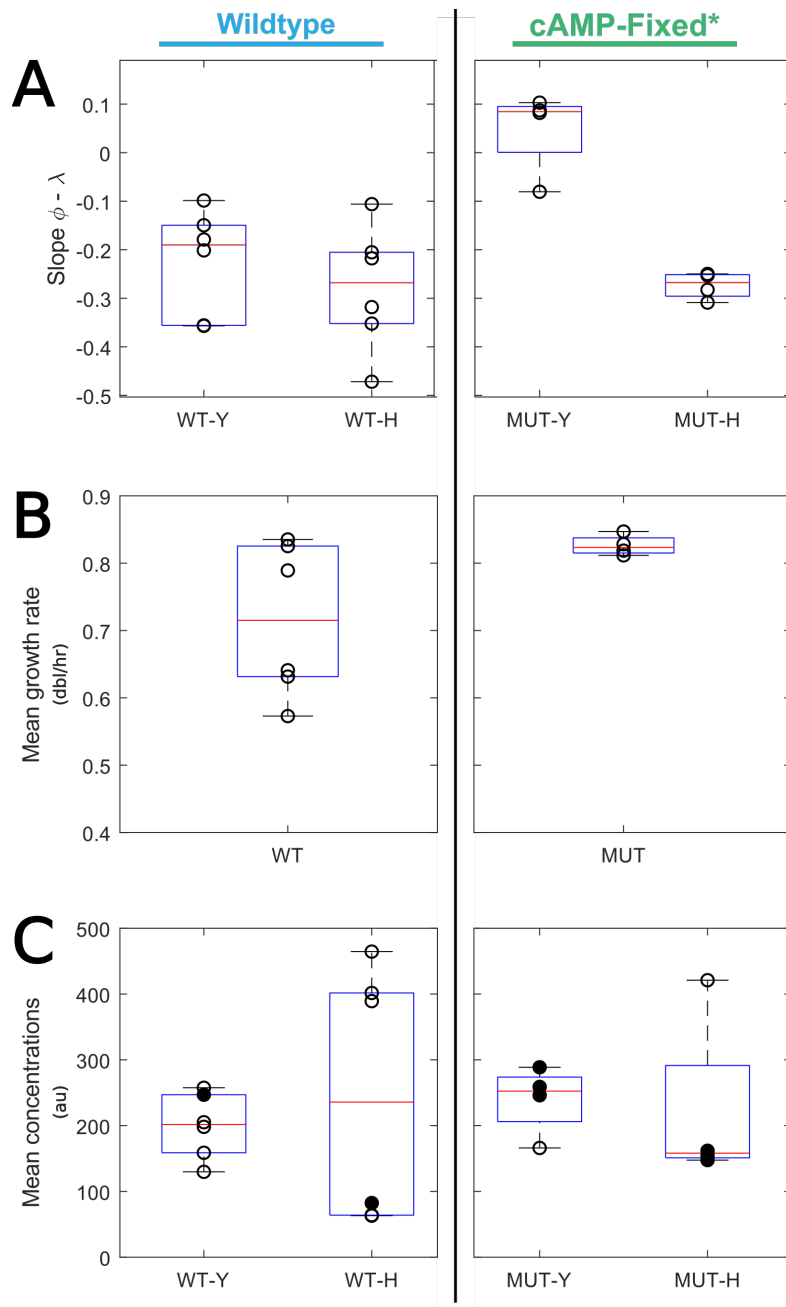


Figure S5: Average experimental values measured in different colonies. **(A)** Regression slope between ϕ and λ for the wild type and cAMP-fixed* cells (MUT in the figure). Slopes for the Y reporter differ significantly between wild type and mutant cAMP-fixed* cells ($p = 0.0031$, two-sample t -test), but not for the H reporter ($p = 0.93$, Welch's t -test). Note that to calculate these regression slopes only relative fluctuations are relevant, so that only relative fluorescence signals are relevant. **(B)** Average growth rate per colony, showing a large variance in growth-rate measurements. Difference between the mean growth rates of WT and cAMP-fixed* cells is not significant ($p = 0.063$, Welch's t -test). **(C)** Average fluorescence per colony. Filled circles are values measured with a standardised microscope setting (and thus only those absolute values can be compared). Y: C-sector reporter, H: constitutive reporter.

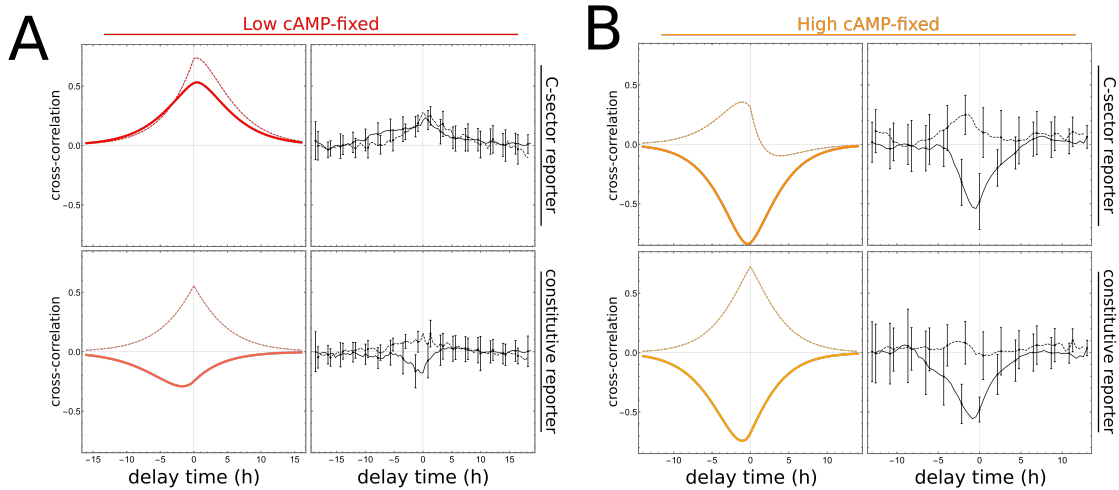


Figure S6: Qualitative model prediction for the cross-correlations as measured in the cAMP-fixed cells using low-cAMP ($80 \mu\text{M}$, panel A) and high-cAMP ($5000 \mu\text{M}$, panel B) conditions, together with the measured cross-correlations. (A) Only the transfer parameters from M to λ ($T_{M\lambda} = 0.6$) and from M to π ($T_{M\pi} = 0.45$) differ compared to the best-fit values from the wild type/cAMP-fixed* condition. (B) Same, but now $T_{M\lambda} = -0.83$, and $T_{M\pi} = -0.47$.

Identifier	Manuscript shorthand	Description
ASC838		Wild type MG1655, also known as strain bBT12 and CGSC number 8003. Known mutations: λ -, Δ fnr-267, rph-1. (No resistance modules.)
ASC839		<i>cyaA</i> , <i>cpda</i> null mutant. Also known as strain bBT80. Based on ASC838. (No resistance modules.)
ASC990	wild type (WT)	Wild type strain, except for $\Delta(\text{galk})::n\text{CRPr-mCerulean-kanR}$ and $\Delta(\text{intc})::\text{CRPr-mVenus-cmR}$. (Kanamycin and chloramphenicol resistant.)
ASC1004	cAMP-fixed	Strain based on ASC839 (ΔcyaA Δcpda), introduced $\Delta(\text{galk})::s70\text{-mCerulean-kanR}$ and $\Delta(\text{intc})::\text{rcrp-Venus-cmR}$. (Kanamycin and chloramphenicol resistant.)

Table S2: Additional details on the strains that were used; ASC990 and ASC1004 were used in the manuscript, and are based on ASC838 and ASC839 respectively.

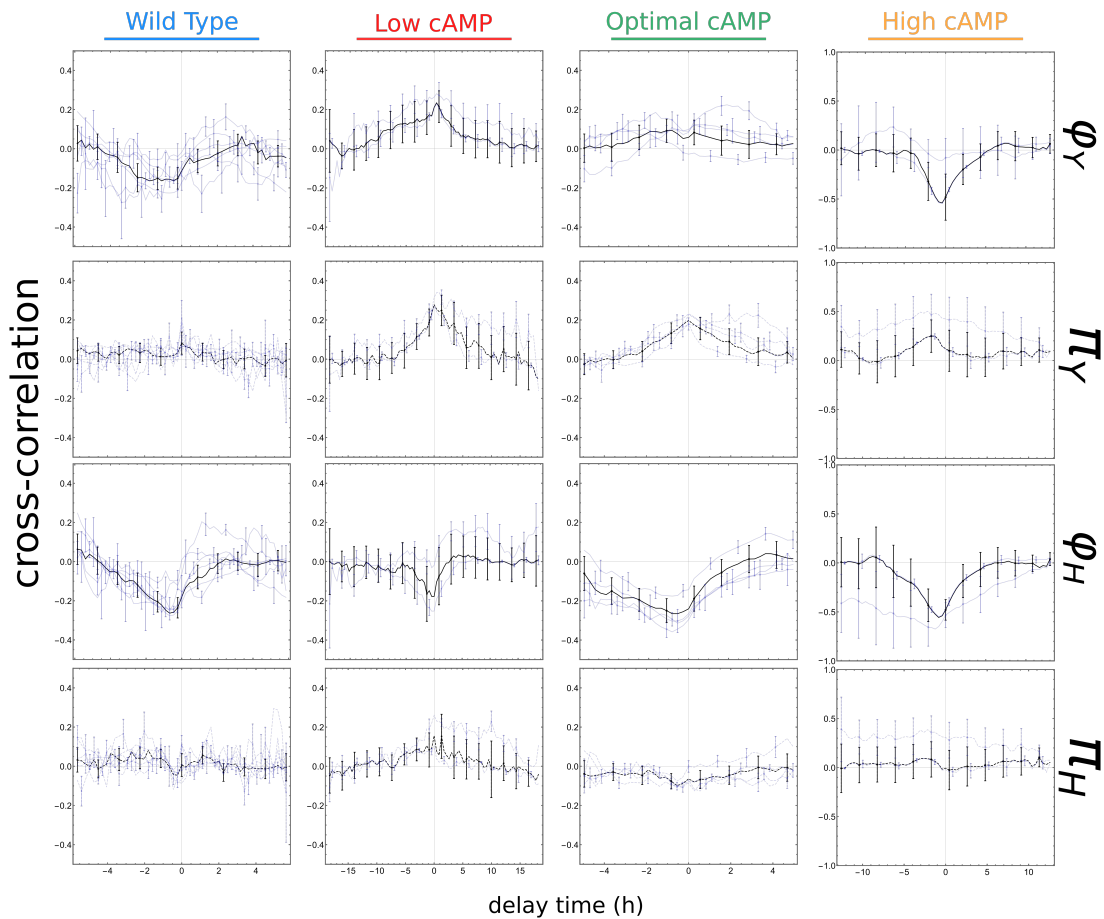


Figure S7: All measured cross-correlations (thin blue lines) in independent replicates (independent colonies), together with their weighted averages (thick black lines), for all conditions. Y: C-sector reporter, H: constitutive reporter.

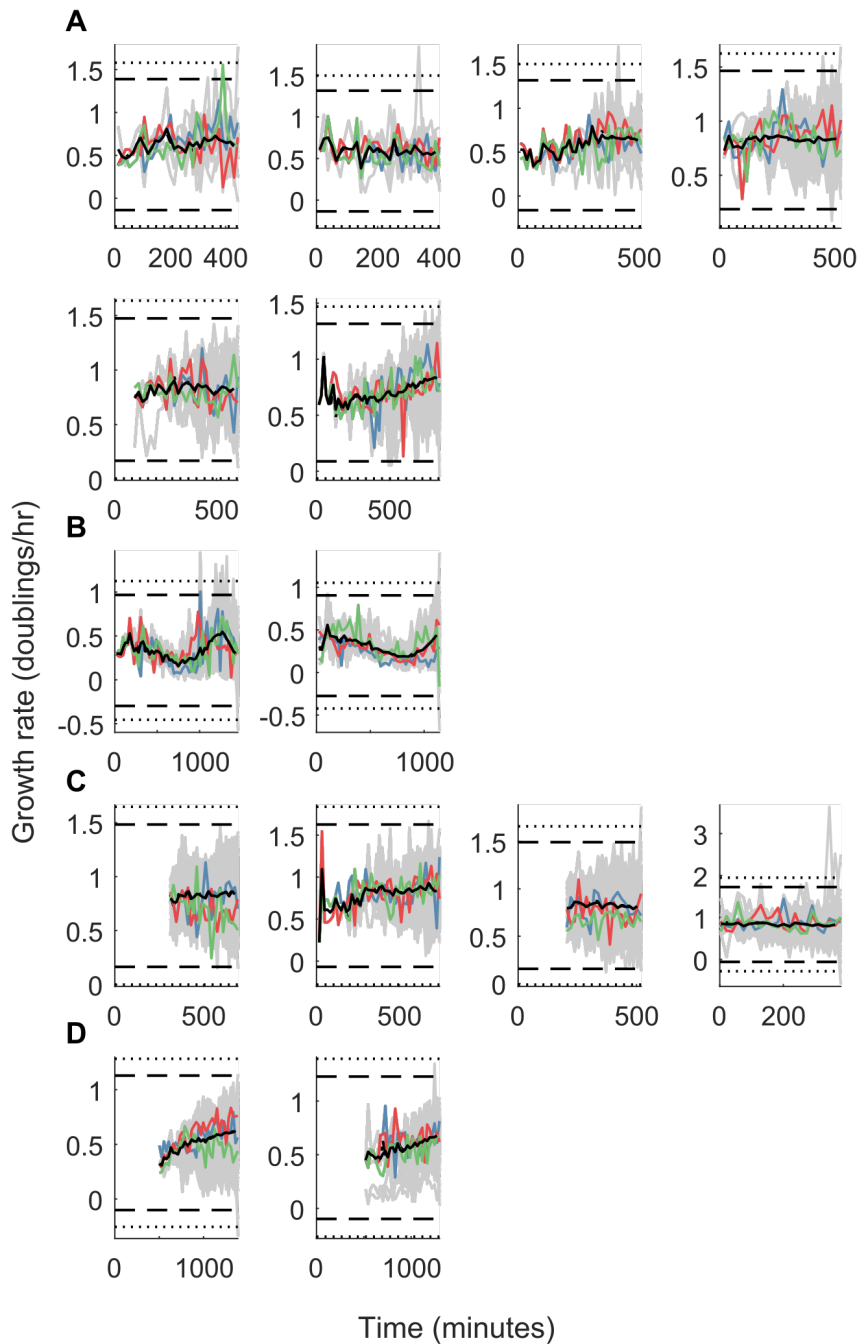


Figure S8: Growth rates during the experiments. Each panel plots growth-rate data for a single colony; panels are grouped by growth condition. The grey lines show single lineage traces, the black lines the population average. Coloured lines highlight example single lineage traces to illustrate single cell behaviour. Dashed and dotted lines indicate 4σ and 5σ boundaries from the overall mean respectively. As before, the displayed conditions are (A) wild type cells, (B) cAMP-fixed* cells growing on 80 μM cAMP, (C) cAMP-fixed cells growing on 800 μM cAMP and (D) mutant cells growing on 5000 μM cAMP.

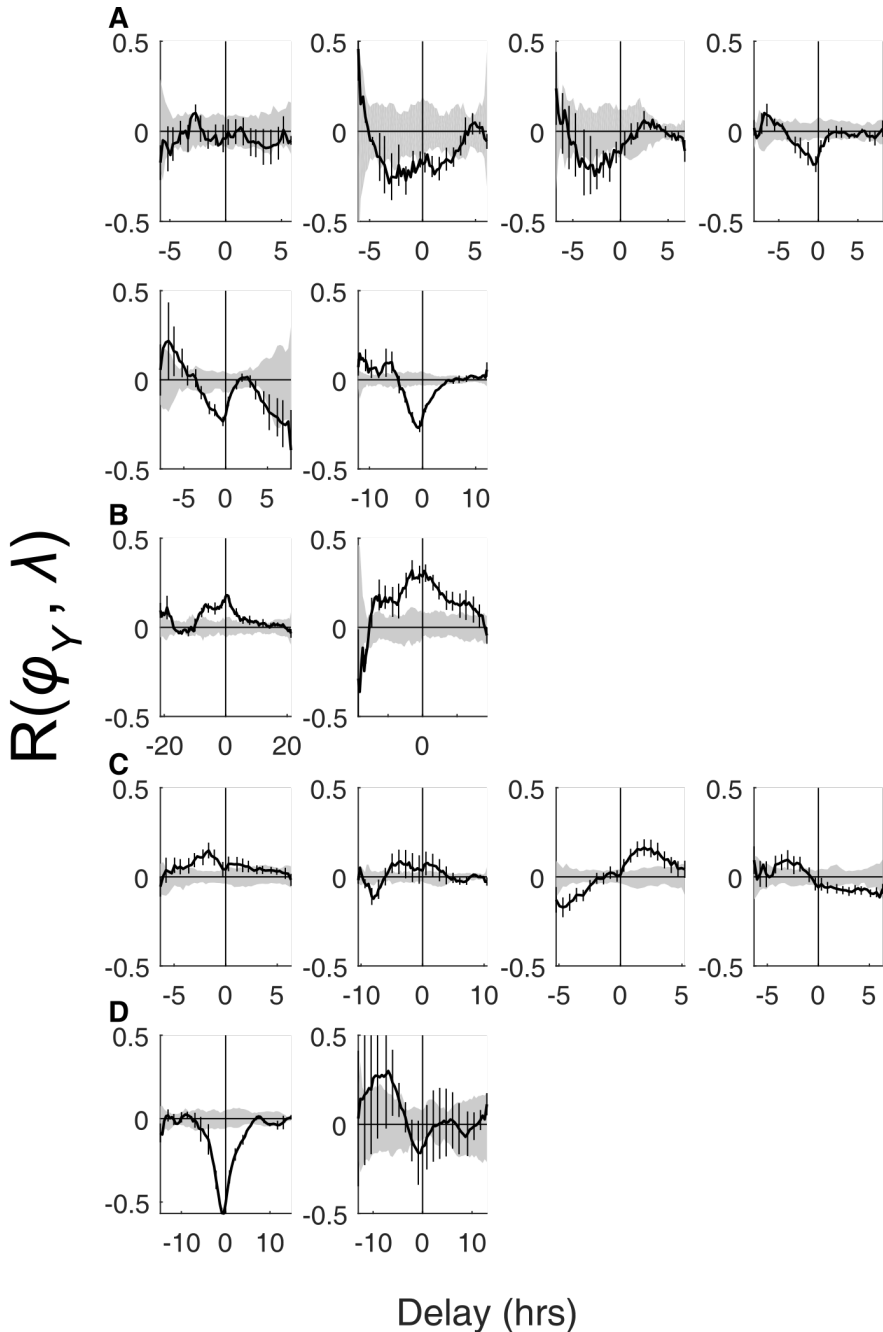


Figure S9: Cross-correlations between the C-sector reporter, ϕ_Y , and λ , together with their null expectation (gray areas around 0, see section 4.3 for details of the calculation). The black lines in this figures are the light-blue lines in top panels of Figure S7. Error bars are calculated by dividing each microcolony into four parts and comparing statistics in each part. As before, the displayed plots are from independent microcolonies growing under the following conditions: (A) wild type cells, (B) cAMP-fixed cells growing on 80 μ M cAMP, (C) cAMP-fixed cells growing on 800 μ M cAMP and (D) cAMP-fixed cells growing on 5000 μ M cAMP.

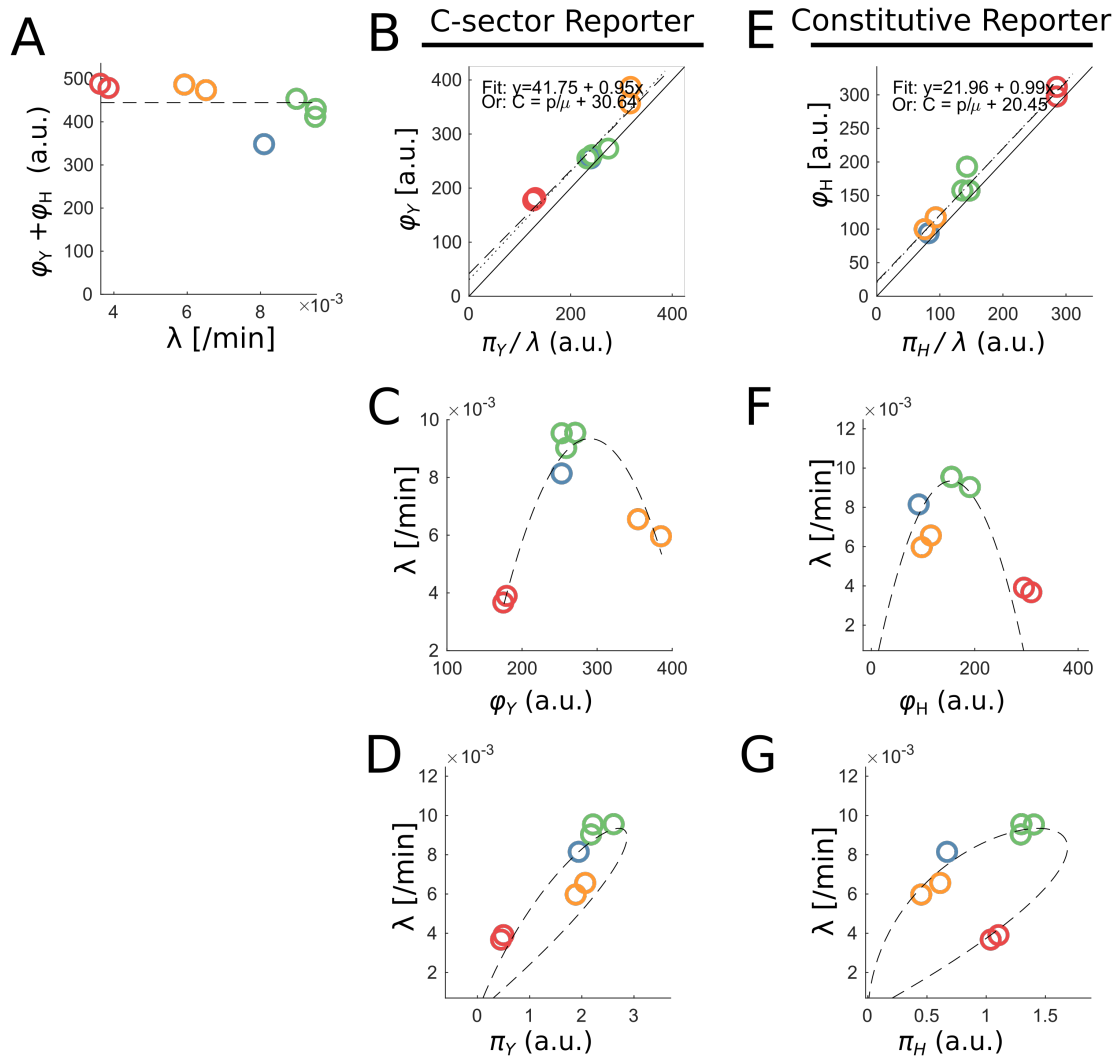


Figure S10: Toy model fits the mean behaviour of the reporters and the growth rate (see for details section 6). (A) The sum of reporter concentrations is approximately constant in all conditions. (B) Steady state relationship $\phi_Y = \pi_Y/\lambda$ (black straight line) holds closely for all conditions. The best fit (dashed line), however, has a slight offset. (C) Fitted parabolic relationship of ϕ_C between the growth conditions. See also S3). (D) Relationship between π_Y and λ as calculated from the toy model (6). (E) Steady state relationship for the C-sector reporter. (F-G) The C-sector reporter concentrations and production rates for each condition fall on the curve calculated from the toy model (not fitted). Colour coding is as in other figures (blue: wild type, red: low cAMP mutant, green: medium cAMP mutant, orange: high cAMP mutant). Y: C-sector reporter, H: constitutive reporter.

PLAC.	GGTTCCGACTGGAAAGCGGGCAGTGAGCGAACGCAATT	AATGT	GAGTTAGCT	CACTC
CRPr.	-----CGTCAGGAGGAGAGGGGCAGTGAGCGAACGCAATT	AATGTGAGTTAGCTCACTC		
nCRPr.	-----CGTCAGGAGGAGAGGGGCAGTGAGCGAACGCAAT	CAGATCAAATGTGTCGTTTC		
pLAC.	ATTAGGCACCCCAGGCTTACACTTATGCTTCCGGCTCGTATGTTGTGTGG	AATTGTGA		
CRPr.	ATTAGGCACCCCAGGCTTACACTTATGCTTCCGGCTCGTATGTTGTGTGCATGGATAA			
nCRPr.	CATAGGCACCCCAGGCTTGACACTTATGCTTCCGGCTCGTATAATGTGTGCATGGATAA			
pLAC.	GC GGATAACAATTTC	CACAGGAAACAGCTATG		
CRPr.	GTAGCTAGGAATTTC	CACACTGCAAACAGCTATG		
nCRPr.	GTAGCTAGGAATTTC	CACACTGCAAACAGCTATG		

Figure S11: Overview of promoter sequences used in this manuscript. The top row indicates the original LacZ upstream region including start codon ATG (NCBI; gene ID 945006, NC_000913.3), whilst the 2nd and 3rd row give the sequence of the engineered CRPr and nCRPr promoters. Colour indicates CRP binding sites according to [6] (yellow), [7] (green) or both (purple), and the LacI binding site (blue) according to [6]. In grey, changes in the engineered promoters are indicated.

References

- [1] D. J. Kiviet, P. Nghe, N. Walker, S. Boulineau, V. Sunderlikova, and S. J. Tans, “Stochasticity of metabolism and growth at the single-cell level,” *Nature*, vol. 514, pp. 376–379, Oct. 2014.
- [2] C. You, H. Okano, S. Hui, Z. Zhang, M. Kim, C. W. Gunderson, Y.-P. Wang, P. Lenz, D. Yan, and T. Hwa, “Coordination of bacterial proteome with metabolism by cyclic AMP signalling,” *Nature*, vol. 500, pp. 301–306, Aug. 2013.
- [3] J. W. Young, J. C. W. Locke, A. Altinok, N. Rosenfeld, T. Bacarian, P. S. Swain, E. Mjolsness, and M. B. Elowitz, “Measuring single-cell gene expression dynamics in bacteria using fluorescence time-lapse microscopy,” *Nature Protocols*, vol. 7, pp. 80–88, Jan. 2012. Bandiera_abtest: a Cg_type: Nature Research Journals Number: 1 Primary_atype: Protocols Publisher: Nature Publishing Group Subject_term: Bacterial physiology;Gene expression analysis;Microscopy;Time-lapse imaging Subject_term_id: bacterial-physiology;gene-expression-analysis;microscopy;time-lapse-imaging.
- [4] L. Susman, M. Kohram, H. Vashistha, J. T. Nechleba, H. Salman, and N. Brenner, “Individuality and slow dynamics in bacterial growth homeostasis,” *Proceedings of the National Academy of Sciences*, vol. 115, pp. E5679–E5687, June 2018. Publisher: National Academy of Sciences Section: PNAS Plus.
- [5] B. D. Towbin, Y. Korem, A. Bren, S. Doron, R. Sorek, and U. Alon, “Optimality and suboptimality in a bacterial growth law,” *Nature Communications*, vol. 8, pp. 1–8, Jan. 2017.
- [6] J. M. Hudson and M. G. Fried, “Co-operative interactions between the catabolite gene activator protein and the lac repressor at the lactose promoter,” *Journal of Molecular Biology*, vol. 214, pp. 381–396, July 1990.
- [7] C. L. Lawson, D. Swigon, K. S. Murakami, S. A. Darst, H. M. Berman, and R. H. Ebright, “Catabolite activator protein: DNA binding and transcription activation,” *Current Opinion in Structural Biology*, vol. 14, pp. 10–20, Feb. 2004.